THE EFFECT OF CRYSTAL STRUCTURE STABILITY ON THE MOBILITY OF GAS BUBBLES IN INTERMETALLIC URANIUM COMPOUNDS*

by

J. Rest, G. L. Hofman, and R. C. Birtcher

Argonne National Laboratory
9700 S. Cass Avenue
Argonne, Illinois 60439

14th International Symposium on
Effects of Radiation on Materials
June 27–29, 1988
Andover, Massachusetts

---

*Work supported by the U.S. Department of Energy.

THE EFFECT OF CRYSTAL STRUCTURE STABILITY ON THE MOBILITY OF GAS BUBBLES IN INTERMETALLIC URANIUM COMPUNDS

by

J. Rest, G. L. Hofman, and R. C. Birtcher

ABSTRACT

Irradiation experiments with certain low-enrichment, high-density, uranium-base intermetallic alloys that are candidate reactor fuel materials, such as U_3Si and U_6Fe, have revealed extraordinarily large voids at low and medium fuel burnup. This phenomenon of breakaway swelling does not occur in other fuel types, such as U_3Si_2 and UAl_3, where a distribution of relatively small and stable fission gas bubbles forms. In situ transmission electron microscope observations of ion radiation-induced rapid swelling of intermetallic materials are consistent with growth by plastic flow. Large radiation enhancement of plastic flow in amorphous materials has been observed in several independent experiments and is thought to be a general materials phenomenon.

The basis for a microscopic theory of fission gas bubble behavior in irradiated amorphous compounds has been formulated. The assumption underlying the overall theory is that the evolution of the porosity from that observed in the crystalline material to that observed in irradiated amorphous U_3Si as a function of fluence is due to a softening of the irradiated amorhpus material. Bubble growth in the low-viscosity material has been approximated by an effective enhanced diffusivity. Mechanisms are included for the radiation-induced softening of the amorphous material, and for a relation between gas atom mobilities and radiation-induced (defect-generated) changes in the material. Results of the analysis indicate that the observed rapid swelling in U_3Si arises directly from enhanced

bubble migration and coalescence due to plastic flow.

I. Introduction

Fission gas bubbles have recently been shown to exhibit extremely high growth rates at relatively low temperatures in certain uranium compounds [1]. It was proposed that this accelerated swelling phenomenon occurs only in compounds that undergo a crystalline-to-amorphous transformation, and that it is a manifestation of radiation enhancement of diffusion and plastic flow in amorphous solids.

The classical model of radiation-enhanced diffusion and creep in crystals, based on the generation of vacancies in excess of their thermal equilibrium concentration, does not apply in a noncrystalline solid where, strictly speaking, the vacant lattice site or vacancy does not exist. In amorphous solids, a model of a radiation-enhanced free volume can be used to interpret the very large flow rates observed. We will draw together here the results of several seemingly unrelated experimental studies in an attempt to generalize this large radiation effect in amorphous solids, and explore a model that describes the effect in particular as it relates to nuclear fuel.

Mineralogists have long recognized the presence of radiation-induced crystalline-to-amorphous transformations in natural radioacative compounds. The extent of this so-called metamict condition is used to determine the age of minerals and was first described by Pellas [2], who showed that partially covalent crystals can undergo this transformation. This bond-type criterion for amorphization has more recently been confirmed in an extensive ion bombardment study of compounds by Naguib and Kelly [3], who fouond that amorphization is quite common and should occur whenever the ionicity is <0.47.

In an attempt to extend the range of compounds in which the metamict condition can be used to determine the age of minerals, Cartz and co-workers [4,5] carried out an ion bombardment and transmission electron microscopy (TEM) study of a number of silicides and nitrides and made some remarkable observations. They found that $ZrSiO_4$ particles irradiated with 1-3.5 MeV Kr ions became amorphous at a dose of 2×10^{19} ions m^{-2}, and that further irradiation caused the non-crystalline particles to bloat into extended disc shapes, quadrupling in diameter at irradiation doses of between 6 and 60×10^{19} ions m^{-2}. A similar large glassy flow occurred in α-quartz after amorphization, whereas Si_3N_4 particles, which remained crystalline after exposure to the same irradiation, retained their original shape and size.

During approximately the same time period, Porter et al. [6] and Fowler et al. [7] studied radiation damage in glass ceramics for fusion reactor applications. They independently observed rapid void or bubble growth in the amorphous phases of these materials under electron bombardment. An example of Porter's observation in the form of time-lapse TEM images, illustrating the rapidity of the growth, is shown in Fig. 1. Void diameter changes estimatged from both Refs. 6 and 7 are similar in magnitude and increase linearly with electron dose. Inferences were also drawn as to the effectiveness of ionization damage, versus the largely displacement damage imposed during previous neutron exposures, in producing bubble growth in ionic crystals. Note that DeNatale and Horwitt [8] have recently observed the same type of radiation-damage phenomenon in previously unirradiated nuclear waste glasses.

The ion bombardment work of Klaumünzer and co-workers is of particular interest because it extends the observation of extraordinarily high radiation-induced growth to

metallic glasses. From a series of papers published from 1982 [9-11], it appears likely that all amorphous alloys (metallic glasses) are susceptible to large plastic flow under heavy ion bombardment. Recently, Klaumünzer et al. performed an ion bombardment experiment with borosilicate glass [12] and again found a very large plastic flow, comparable to that seen in the metallic glasses.

In reactor irradiation experiments with intermetallic uranium compounds, Hofman [1] showed that an enormous increase in gas bubble growth occurs when a compound becomes amorphous during irradiation. An example of this rapid bubble growth in U_3Si is illustrated in Fig. 2. Evidence of very large plastic flow in neutron-irradiated materials has also been reported in U_6Fe by Bloch [13], in PU_6 Fe by Coffinberry and Waldron [14] and in BeO by Yeniscavich and Bleiberg [15]. In every one of these experiments, the material exhibiting excessive flow was found to be amorphous after irradiation.

Finally, the ion bombardment and in situ TEM experiments of Birtcher et al. on U_3Si [16] underscore the general nature of the effect. During irradiation of the amorphous phase, the initial specimen perforation increased rapidly in size. This did not occur in the crystalline phase. Figure 3 shows the behavior of a strip of material between two holes in amorphous U_3Si during 1-MeV Kr irradiation. This material is under tension during the irradiation and undergoes plastic flow. Small holes within the strip grow and coalesce. This growth stops when the irradiation is interrupted. The overall behavior is identical to that displayed by reactor-irradiated U_3Si (Fig. 2). These observations suggest that plastic flow induced by a large radiation dose is not restricted to partially covalent materials but can occur in any amorphous solid.

The deformation measurements obtained in the ion bombardment experiments of Cartz, Klaumünzer, and Birtcher are combined in the plot shown in Fig. 4. The close grouping of the data should be considered coincidental and not indicative of a functional relationship, since no corrections for experimental differences have been made. However, Fig. 4 does illustrate the magnitude of observed deformations as well as the apparent linear relationship between deformation and irradiation dose. This linear dose dependence, which was also found during the electron irradiations of Porter and Fowler, indicates that atomic displacements control the deformation rate.

This summary of results of widely different experiments strongly suggests a unique radiation effect in glassy materials. The very large plastic flows suggest low viscosities characteristic of glass near its softening point. However, all experiments were performed below 0.3 T_m, temperatures where the materials in question are hard and have high viscosities. Indeed, after irradiation these amorphous materials are found to be hard and brittle. For example, the microhardness of U_3Si (measured after irradiation), increased slightly after prolonged neutron irradition, during which the compound became amorphous and experienced excessive swelling. The drastic difference between elastic properties during and after irradiation is graphically shown in Fig. 5, which is a scanning electron microscope (SEM) image of the surface of a large fission gas bubble in U_3Si. The smooth flow patterns on the bubble surface indicate viscous behavior, whereas the fractured "ligaments" which had connected two sides of the bubble, and which were broken during SEM sample preparation after irradiation, indicate brittle behavior. It may be concluded that viscous flow occurs under ion, electron, and neutron irradiation and fissioning in the glassy (amorphous) state only, whether this state is pre-existing or is formed during the irradiation.

As suggested in the proceding discussions, the underlying mechanisms affecting swelling behavior in intermetallic compounds involve mechanical instability under irradiation. As we shall show, radiation-enhanced diffusion and plastic flow are key determinants of swelling behavior. Figure 6 is a plot of the fuel swelling, obtained from immersion density measurements, for U_6Fe, U_3Si, U_3Si_2, and UAl_3 dispersion fuels. The UAl_3 and U_3Si_2 show little swelling after very high U burnup, but the higher density U_6Fe and U_3Si experience rapid swelling at medium and low burnup.

The differences in fission gas bubble behavior are illustrated in Fig. 7 for the four fuels shown in Fig. 6. Typically, UAl_3 does not develop resolvable fission gas bubbles, but U_3Si_2 contains bubbles which have an extremely narrow size distribution and uniform spacing, and which appears to be arranged in rows. The U_3Si develops large bubbles which interconnect and result in rapid swelling. At low burnup, U_6Fe likewise develops large irregular bubbles which interconnect, causing a sharp increase in the swelling curve. As will be shown in Section II, the swelling behavior of the stable compounds UAl_3, U_3Si_2, and USi can be explained with current models of fission gas behavior in nuclear fuels, models that include such effects as radiation-enhanced diffusion and nucleation and growth of fission gas bubbles on grain boundaries, subgrain boundaries and dislocations in a crystalline solid.

In Section III, it will be shown that the gas bubble growth observed in U_6Fe, U_3Si, and U_6Mn at low temperature can be explained by assuming that under irradiation, properties of the fuel approach those of the liquid state. Results will be presented which suggest that extraordinarily low viscosity occurs in amorphous solids under irradiation. An

analytical model will be presented which relates the migration energy for diffusion within a defect cascade to the level of damage sustained in the material. Measurements by Okamota et al. [17] of the change in sound velocity in irradiated intermetallic compounds have shown that substantial elastic softening of the intermetallic compounds occurs in the crystalline state and is associated with the progressive destruction of the chemical long-range order which precedes the onset of amorphization in these materials. The shear constant decreases linearly by as much as 50% with increasing volume dilation, and extrapolates to zero at a volume dilatation of about 4.7%.

II. Fission Gas Bubble Behavior in Crystalline Intermetallic Compounds

A. Models

Estimates of the quantity of gas that can be accounted for in the observed U_3Si_2 bubble population (Fig. 7) fall far short of the total amount generated. As the limit of resolution in the SEM is about 50 nm, it is likely that a high density of small bubbles and/or a high concentration of gas in solution is present within the U_3Si_2 matrix. A mechanistic fission gas release and swelling mode, GRASS-SST [18,19], has been utilized to interpret the observations.

For the purpose of calculation (i.e., reasonable code running times), the bubbles are represented by a set of size classes defined in terms of the number of gas atoms per bubble. This method of grouping significantly reduces the number of equations needed to describe the bubble size distributions. The bubble classes are ordered so that the first class refers to bubbles that contain only one gas atom. If S_i denotes the average number of atoms per bubble for bubbles in the ith class (henceforth, called i bubbles), then the bubble

size classes are defined by

$$S_i = mS_{i-1} \tag{1}$$

where $m \geq 1.6$, $i \geq 2$, and $S_1 = 1$. The S_1 class is assumed to consist of a single gas atom associated with one or more vacancies or vacancy clusters. P_{ij} is the probability of an i bubble coalescing with a j bubble when the bubbles move by random motion, and is given by

$$P_{ij} = 4\pi(r_i + r_j)(D_i + D_j) \tag{2}$$

where r_i is the average i-bubble radius and D_i is the average i-bubble diffusion coefficient in the lattice.

The rate of coalescence, C_{ij}, of bubbles with j bubbles is given by

$$C_{ij} = P_{ij}F_iF_j \tag{3}$$

where F_i is the number of i bubbles per unit volume. Details of the bubble growth calculation are given in the Appendix.

Dislocations can act as trapping sites for fission gas and bubbles. The fission gas atoms diffuse by random motion to dislocations at a rate

$$R^d = \frac{2\pi D_1 \rho c}{ln(r_c/r_i)} \tag{4}$$

where ρ is the dislocation density, c is the concentration of fission gas in the lattice, r_1 is the radius of a single gas atom, and r_c is the radius of the cylindrical capture volume around the dislocation, i.e.,

$$(\pi r_c^2)\rho = 1. \tag{5}$$

Once the fission gas is pinned to dislocations, the gas can coalesce with both lattice and dislocation bubbles (re-solution causes gas atoms to be knocked back into the lattice). Coalescence probabilities for bubbles on dislocations can be derived from a solution of the one-dimensional, time-dependent diffusion equation, and are given by

$$P_{ij} = (D_i^d + D_j^d)/\sqrt{\rho}, \tag{6}$$

where D_i^d is the average i-bubble diffusion coefficient on dislocations.

Bubble growth in crystalline U_3Si_2 during low-temperature (<200°C) irradiation occurs primarily by the diffusion of gas atoms to existing bubbles, i.e., the bubbles are basically immobile. Gas atom diffusion in U_3Si_2 at 100°C is primarily athermal, i.e., irradiation enhanced. The gas atom diffusivities used in GRASS-SST are taken from those reported by Höh and Matzke [20], and are given by

$$D_a = 3.5 \bullet 10^{-40} m^5 \bullet f \tag{7}$$

where f is the fission rate.

Bubble growth is limited not only by the gas atom and gas bubble densities and diffusivities, but by radiation-induced gas atom re-solution, i.e., the rate, b, at which gas atoms are ejected from a bubble owing either to direct or to indirect collisions by fission fragments.

The re-solution rate is calculated with the assumption that gas atom re-solution from a spherical bubble is isotropic and proceeds by the knocking out of single gas atoms. Thus, from geometrical considerations

$$b_i = \frac{2b_o f}{r_i^3} \int_{r_i - \lambda}^{r_i} \left(\frac{1 + \cos\theta_i}{2}\right) R^2 \, dR \tag{8}$$

where $\cos\theta = (r_i^2 - \lambda^2 - R^2)/2R\lambda$, λ is the distance an average ejected atom travels, and b_o is an experimentally determined constant [19].

For bubbles on dislocations, equilibrium is reached when the diffusion flux of gas atoms from the local concentration gradients is balanced by the flux owing to re-solution. If instantaneously there are N_i bubbles per unit length of dislocation, the re-solution flux is $N_i b/2$. If the gas atom concentration is zero at the dislocation and C^λ a distance λ from it, the diffusion flux is approximately given by $D\, C^\lambda/\lambda$ from Fick's law. Thus, at equilibrium, when the two fluxes are equal.

$$(1 - C^\lambda/C^\circ) = 1 - \sum_i N_i b_i \lambda/2DC^\circ \tag{9}$$

where C° is the gas atom concentration far from the dislocation.

Within the rate theory approach used in GRASS-SST, the rate of gas atom re-solution from dislocation bubbles, $bN_i/2$, is multiplied by the factor $C_o^\lambda = C^\lambda/C^\circ$ to obtain the backward flux of gas atoms. Good agreement between theory and experiment is obtained only for small values of C_o^λ ($C_o^\lambda << 1$). Physically, these results are interpreted as due to a small value of the penetration depth, λ. The value of λ used in GRASS-SST ($\lambda = 5$ nm) and by Dowling et al. [21] is consistent with this conclusion and is on the order of a defect cascade size.

A system of coupled equations for the evolution of the size distribution of fission gas bubbles in the lattice and on dislocations can be derived [19] on the basis of the models discussed above. The equations have the form

$$F_i^\alpha = - A_i^\alpha F_i^\alpha F_i^\alpha - B_i^\alpha F_i^\alpha + C_i^\alpha (i = 1, \ldots, N;\ \alpha = 1,2) \tag{10a}$$

where F_i^α is the number of α-type bubbles in the ith size class per unit volume; α = 1,2 represents the lattice and dislocation distributions, respectively; and the coefficients B_i^α and C_i^α obey functional relationships of the form

$$C_i^\alpha = C_i^\alpha(F_i^\beta, ..., F_{i-1}^\beta, F_i^\alpha, F_{i+1}^\beta ..., F_N^\beta) \tag{10b}$$

$$B_i^\alpha = B_i^\alpha (F_1^\beta, ..., F_{i+1}^\beta, F_i^\alpha, F_{i+1}^\beta ..., F_N^\beta)$$

where $\alpha = 1; \beta = 1,2; \alpha = 2$

$\alpha = 2; \beta = 1,2; \alpha = 1.$

In Eq. 10, A_i^α represents the rate at which α-type bubbles grow out of the ith size class due to coalescence with other bubbles in the ith class; B_i^α represents the rate at which α-type bubbles are lost from the ith size class owing to coalescence with bubbles in other size classes, change in bubble type owing to bubble migration processes, and re-solution; and C_i^α represents the rate at which bubbles are being added to the ith size class owing to fission gas absorption, bubble nucleation, bubble growth resulting from bubble coalescence, and bubble shrinkage from the i+1 class due to gas atom re-solution.

Figure 8 is a GRASS-SST flow chart. Given the operating conditions, such as the time step, temperature, stress, grain size and dislocation densities, GRASS-SST calculates the equilibrium bubble radii for the size classes of bubbles under consideration (the initial number of size classes is an input) by using a modified hard-sphere equation of state for xenon as well as the generalized capillary relation

$$P_i(T) = \frac{2\gamma}{r_i} + \sigma_H \tag{11}$$

where $P_i(T)$ is the gas pressure in a bubble with radius r_i, γ is the surface energy, and σ_H is the local hydrostatic stress.

After the bubble radii have been determined, the bubble diffusivities and coalescence probabilities are calculated. The code then solves for the bubble size distributions (Eqs. 10) incrementally by using a modified midpoint rule to generate a sequence of approximations; every sequence is interpolated by rational functions to obtain a "trial" solution until specified convergence criteria are satisfied. (If required, the code will increment the number of size classes involved in the calculation.) Finally, the fission gas released and the swelling due to retained gas are calculated. The intragranular swelling due to retained fission gas is calculated from the bubble size distributions, F_i^{α}, using

$$\Delta V = \frac{4\pi}{3} \sum_{i,d} r_i^3 \, F_i^{\alpha} \qquad (12)$$

B. Results of GRASS-SST Calculations

The observed bubble distribution in crystalline U_3Si_2 contains bubbles having a relativey uniform separation, with many of the bubbles lying along straight lines (Fig. 7). Electron microscope observations of intragranular bubble distributions in uranium dioxide irradiated at temperatures in excess of about 700°C have also shown bubbles lying in straight lines [22]. Calculations of homogeneous bubble nucleation suggest that heterogeneous nucleation is most likely to occur when nuclei are present with a spacing of less than a micron [23]. This led Speight [24] to the supposition that dislocations or, more likely, dislocation networks that form low-angle subgrain boundaries act as favorable nuclei for bubble growth under these conditions, since they are present on this scale and their

effective binding energy with fission gas atoms is large. Studies of helium precipitation in metals have shown directly that He precipitates at dislocations [25]. In fissile materials, it would appear that as the bubbles nucleate and grow, their associated dislocations will climb by adsorption of excess interstitials remaining after vacancies are absorbed by bubbles and other sinks (equal numbers of vacancies and interstitials are produced). The climb is such that a bubble transfers from the tensile to the compressive side of the dislocation and away from the region of high gas density. The only locations that remain as good nucleation and growth centers throughout the irradiation are the dislocation nodes, and it is to be expected that the largest bubbles will be located at these sites, with small ones on or near dislocation lines.

Figure 9 shows the GRASS-SST-calculated bubble size distribution in U_3Si_2 at 16 U at.% burnup. Also shown is the average observed bubble diameter. The calculation shown in Fig. 9 was made with the assumption that gas atom re-solution from bubbles on dislocations is a factor of 10 smaller than re-solution of bubbles in the lattice. This difference is due to a larger knock-out distance required to separate a gas atom from a bubble located on a dislocation. For gas-atom knock-out distances, λ, less than the gas-capture radius for a dislocation, r_c, the gas associated with bubbles on dislocations is effectively trapped. Thus bubbles on dislocations grow at a faster rate. As can be seen from Fig. 9, the GRASS-SST-calculated distribution of bubbles on dislocations is in good alignment with the average bubble diameter. The majority of the generated fission gas is predicted to be in very small bubbles not on dislocations (radii less than about 5 nm). However, the small bubbles are responsible for only 50% of the total swelling.

Figure 10 compares the measured and GRASS-SST-calculated gas bubble swelling as a function of fluence for U_3Si_2. The calculation closely matches the linear

dependence of the observed swelling on fluence. The constant difference between the straight-line approximation to the data and the GRASS-SST-calculated values can be associated with solid fission products (i.e., fission products other than the noble gases) not included in the GRASS-SST calculations. Sensitivity studies performed with GRASS-SST indicate that the calculated results shown in Fig. 9 are relatively insensitive to the value of the athermal diffusivity, D_a, and the assumed value for the dislocation density, ρ. However, the size distribution of bubbles on dislocations is very sensitive to the assumed value for the dislocation gas atom re-solution rate, i.e., b_0 in Eq. 8. The reason for the relative insensitivity to D_a of the calculated distribution of bubbles on dislocations and in the lattice is related to the dominance of re-solution of gas atoms originally contained within highly concentrated bubbles in the lattice. The motion of gas in the lattice is dominated by a high number of trapping (by bubbles) and detrapping (via re-solution) events. Increasing D_a increases the gas atom mobility while at the same time increasing the trapping rate at small bubbles in the lattice. These two interrelated and competitive processes result in a relatively weak D_a dependence of the gas atom flux to dislocations.

On the other hand, the gas atom re-solution rate from dislocation bubbles directly affects the growth rate of the bubbles on dislocations. A decreased value for the dislocation gas atom re-solution rate allows the dislocation bubbles to effectively retain their gas. Reasonable agreement is obtained for re-solution from dislocation bubbles at a rate that is a factor 10 lower than that used for bulk gas atom re-solution. This observation is consistent with the gas atom capture properties of dislocations.

III. FISSION GAS BUBBLE BEHAVIOR IN IRRADIATED AMORPHOUS INTER-METALLIC COMPOUNDS

As discussed in Section I, observations of certain low-enrichment, high-density, uranium-base intermetallic alloys, such as U_3Si and U_6Fe, have revealed extraordinarily large voids at low and medium fuel burnup. This phenomenon of breakaway swelling does not occur in other fuel types, such as U_3Si_2 and UAl_3, where instead a distribution of relatively small, stable fission gas bubbles forms. The in situ observations of ion-radiation-induced rapid swelling of intermetallic materials (see Fig. 3) are consistent with growth by plastic flow.

A microscopic theory of fission gas bubble behavior in irradiated amorphous compounds is proposed in this section. The assumption underlying the overall theory is that the difference in evolution of the porosity between crystalline and amorphous U_3Si is due to a softening of the irradiated amorphous material with a concurrent orders-of-magnitude increase in the effective gas bubble diffusivity due to plastic flow. The coupling of changes in shear modulus with radiation-induced softening of amorphous material and gas atom mobility within defect cascades is discussed.

A. Model for Irradiation-induced Softening of Amorphous Materials

The major differences between the crystalline and amorphous phases are due to changes in the elastic properties. In a number of recent studies discussed in Section I, elastic softening of irradiated glasses was reported. P. R. Okamoto et al. [26] show that substantial elastic softening of intermetallic compounds occurs in the crystalline phase and is associated with the progressive destruction of the chemical long-range order. Brillouin scattering experiments and transmission electron diffraction studies [27] have shown that

single-crystal silicon and polycrystalline intermemtallic compounds undergo dramatic elastic softening after irradiation with charged-particle beams. Measurements of the change in sound velocity show that the average shear constant decreases by as much as 30% in silicon and by as much as 50% in intermetallics. These results point to a strong coupling between strain and order parameter as a possible origin of the elastic softening and to strain accumulation as an important prerequisite for the amorphization of these intermetallics.

The degree of long-range atomic order, S, has an exponential dependence on the total dose ϕt,

$$S/S_o = \exp(-K\phi t). \tag{12}$$

Measurements by Okamoto et al. [17] of the Zr_3Al lattice dilation, $\Delta a/a$, determined from the change in spacings of the (400) fundamental reflection, showed that $\Delta a/a$ increases with increasing dose, reaches a maximum value of about 0.8% at the dose where amorphization starts, then drops abruptly to ~0.7% (S~0) and thereafter remains approximately constant. For doses up to 0.2 dpa, the percentage lattice dilatation is a quadratic function of S:

$$\Delta a/a = (\Delta a/a)_m [1 - (S/S_o)^2] \tag{13}$$

where $S/S_o = \exp[-11.6\ \phi t]$ is the observed dose dependence of S and $(\Delta a/a)_m = 0.775\%$ is the maximum lattice dilatation due to disordering. The results of Brillouin scattering measurements (post-irradiation) on the same material showed that a large (~50%) decrease in the shear constant occurs after chemical disordering. The decrease occurs prior to the onset of amorphization, and hence the elastic softening is a precursor effect rather than a consequence of amorphization. This result is significant since it strongly suggests that an elastic instability triggers the onset of amorphization. For doses up to 0.15 dpa, the shear

constant is a quadratic function of S:

$$C/C_0 = 0.5\,[1 + (S/S_o)^2]. \qquad (14)$$

The S^2 dependence of both the elastic softening and lattice dilatation can be understood-qualitatively in terms of phenomenological theories of order-disorder based on central pair-wise interactions, as described in Refs. 12 and 13 of the paper by Okamato et al. [26].

The S^2 dependence described by Eqs. 13 and 14 implies that the shear constant is a linear function of volume dilation, $3\Delta a/a$. Eliminating $(S/S_o)^2$ in Eqs. 13 and 14 yields

$$C/C_o = [1 - (3\Delta a/a)/4.65]. \qquad (15)$$

As described by Eq. 15, the shear constant decreases linearly with volume dilatation and extrapolates through the glass gap (i.e., the change in the density between the partially disordered crystalline phase and the amorphous phase is ~2.5% to zero at $3\Delta a/a$ (~4.7%), which is very close the value of $4 \pm 1\%$ measured by Schulson for total volume expansion of amorphous Zr_3Al [28]. The loss of resistance to shearing at a dilatation of 4.7% indicates that the partially disordered material ($S \sim 0.2$) is mechanically unstable with respect to density fluctuations comparable in magnitude to the glass expansion gap. Since density fluctuations of comparable magnitude may occur in the cores of energetic cascades, the irradiation itself can provide the additional density fluctuation required to trigger an elastic instability in the partially disordered material. An estimate of these density fluctuations in U_3Si is presented inSection IIIC.

Okamoto et al. [26] emphasize that the elastic instability which occurs during irradiation is not one in which the entire crystal transforms catastrophically to an amor-

phous phase at some critical disorder. The glass expansion gap represents a nucleation barrier against glass formation in the highly-strained, metastable, disordered crystalline material. Although the dilatational strain will have a well-defined average value, local dilatation fluctuations result in regions of mechanical instability, i.e., amorphization, and not everywhere simultaneously. In the context of the theory being developed in this paper, the important point is that disorder results in a volume-dependent shear coefficient during irradiation similar to that associated with the heating and melting of metals.

B. Calculation of Gas-Atom Diffusivities Within Defect Cascades

Measurements of ion beam mixing of tracer impurities in metallic glasses and in the pure crystalline elements comprising the glasses performed by Hahn et al. [29] at 80 K demonstrated that the ion mixing efficiency of the tracer impurities was greater in the metallic glasses than in either of the constituent elements for the NiZr and CuEr systems. The athermal diffusivities of the tracer impurities in the metallic glasses was within a factor of 10 of those measured in the crystalline materials. Although in the right direction, a factor of 10 increase in the gas-atom diffusivities is not sufficient to explain the breakaway swelling observed in the irradiated U_3Si material (Fig. 2). However, the Hahn et al. results are consistent with the picture of cascade dynamics provided by recent molecular dynamics computer simulations [30]. The simulations show that the cascade region has a "liquid-like" structure during the thermal spike phase of the cascade evolution.

C. P. Flynn [31] has developed a simple picture for the relationship between the migration energy for diffusion and the elastic constants of the material. A diffusion jump introduces a lattice strain. One may expect the strain caused by the jump to be mainly a shear. An estimate of the energy in this shear strain can be obtained by treating

the material as a Hookeian solid. For Hookeian shear, the work done per unit volume of strain energy in the body is given by

$$W = \frac{1}{2}\,\varepsilon^2 C' \tag{16}$$

where C' is the shear modulus and ε is the strain caused by the jump. The energy in the shear strain is obtained by multiplying W by the strained volume. Choosing a volume given by $\frac{4}{3}\,\pi a^3$, where a is the atomic spacing, results in

$$E_m = \frac{4}{3}\,\pi a^3 C'\varepsilon^2 \tag{17}$$

In Flynn's more rigorous elastic theory, large atomic displacements causing diffusion jumps in monatomic crystals are treated as a summation of phonon amplitudes. Using the harmonic approximation, Flynn derived an expression for a Gibbs function for the migration energy given by

$$E_m = C\,\Omega\,\delta^2 \tag{18}$$

where C is an average elastic constant for migration, Ω is the atomic volume, $\delta^2 = q^2/s^2$, where q measures the energy fluctuation needed for a jump to continue to completion and s is a measure of the jump path. Equations 17 and 18 have the same functional dependence on the shear modulus. A decrease in the shear modulus will result in a proportional decrease in the migration energy for diffusion.

The thermally activated gas atom diffusivities in the amorphous phase can be described by an exponential dependence on tempreature, i.e.,

$$D_a = D_o \exp(-E_m/RT). \tag{19}$$

Gas atom mobility in irradiated crystalline material at relatively low temperatures is dominated by athermal diffusion. However, a decrease in E_m may result in thermal activation dominating the diffusion process. From Eqs. 18 and 15, the migration energy in the damaged material is reduced to

$$E_d = E_m [1 - (3\Delta a/a)/4.65] \tag{20}$$

where E_m is on the order of the migration energy in the undamaged material. The diffusivity in the damaged material is thus increased to

$$D_d = D_a \exp [(E_m/RT) \bullet (3\Delta a/a)/4.65]. \tag{21}$$

For a 3% dilatation, the diffusivity at 150°C would be enhanced by about ten orders of magnitude over thermal diffusion.

It is important to note that the gas atom diffusivity as given by Eq. 21 is appropriate only for local regions of the amorphous (or crystalline) material which are sustaining damage. The dilatation, $\Delta a/a$ in Eq. 21, applies to this damaged region (e.g., the volume of the damage cascade), and is estimated to have a lifetime on the order of the defect cascade, 10^{-10} s. From the analysis presented in section III A on the irradiation-induced softening of amorphous materials, it follows that Eq. 21 applies as well to damaged regions in partially disordered crystalline materials. The key difference in bubble behavior between irradiated crystalline and amorphous materials suggested by the experimental results presented in section I is that the amorphous materials can undergo substantial plastic flow. In irradiated amorphous materials containing fission gas (e.g., U_3Si), overpressurized bubbles can provide the driving force for flow. In addition, density fluctuations produced by the damage cascade can provide a driving force for microscopic deformation. Plastic flow, in turn, results in enhanced bubble coalescence and bubble sweeping of gas

atoms out of solution.

The calculation of bubble growth in irradiated amorphous materials is complicated by the interplay between bubble growth (driven by plastic flow) and plastic flow (e.g., driven by bubble overpressure). In order to provide for a computationally tractable description of this phenomenon, the assumption is made that bubble motion in a material undergoes plastic flow can be described by an effective bubble diffusivity on the basis of random motion in a liquid where the bubbles move by volume diffusion. The diffusivity of a bubble of radius r_i migrating by volume diffusion is given by

$$D_i = \frac{3\Omega}{4\pi r_i^3} D_u \tag{22}$$

where Ω is a molecular volume and D_u is the diffusivity of the diffusing atoms. This diffusion is qualitatively described by the Stokes-Einstein equation:

$$D_u = kT/(6\pi r_u \eta) \tag{23}$$

where r_u is the radius of the diffusing species and η is the viscosity. A softening of the material produces a decrease in η and a corresponding increase in D_u. The assumption is made here that in irradiated amorphous materials, the effect of plastic flow can be described by using an effective atomic diffusivity D_u equal to D_d (Eq. 21).

C. Results of GRASS-SST Calculation

The reader should keep in mind that several key physical processes are occurring simultaneously as damage is sustained in the material. The first process is radiation-induced crystalline to amorphous transitions, which occur in certain materials when long-range order in the crystal is destroyed. The loss of long-range order, directly

observed by Okamoto et al. [26], has been qualitatively correlated with compound stability, as expressed by the free energy of formation [1]. The amorphization process occurs on a microscopic scale when the local dilatation due to a damage cascade exceeds the glass expansion gap. Subsequently, the number density of these microscopic amorphous regions increases with time until they begin to overlap. The dose dependence of the amorphous volume fraction can be estimated by using a statistical overlap model [32] which assumes that each fission event produces many cascades that are amorphous.

The second process is the softening of the amorphous regions. This irradiation-induced softening process was noted by Klaumunzer [9-11] and others [4,5], and can be understood in terms of local density fluctuations which increase the free volume. Bethune [33] has observed an anomalous volume increase of 2.4% in U_3Si irradiated at temperatures below 100°C. Although he has interpreted his observations in terms of small vacancy clusters of diameter < 2 nm, they could be interpreted as an overall increase in free volume.

The third process is the increase in the motion of gas bubbles in material undergoing plastic flow. This motion has been qualitatively described by the use of effective atomic mobilities in the irradiated amorphous regions as described by Eq. 22. (Note that these atomic mobilities are directly applicable to the damage cascade region.) The increased atomic mobilities result in an enhanced growth rate of small gas bubbles and a reduction in the effectiveness of gas atom re-solution. The resultant overpressurized bubbles provide a driving force for plastic flow. Subsequently, the growing bubbles interconnect and the result is substantial porosity and deformation.

Approximately 5 MeV of damage energy is liberated by each fission event, and each event consists of about 200 cascades having individual energies of 5 to 30 keV. The increase of the amorphous volume fraction, V_A, is given by

$$\frac{dV_A}{dn} = V_c\,[1-V_A] \tag{24}$$

where V_c is the average cascade volume and n is the number of cascades produced. Integrating Eq. 24 yield

$$V_A = 1 - \exp[-V_c n] \tag{25}$$

For a fission rate of 1×10^{21} $m^{-3}s^{-1}$ and cascades with diameters of 10 nm, the material will be 99 percent amorphous after a dose of 4.4×10^{22} fissions$\cdot m^{-3}$ or a time of 45 sec. Within a relatively short time the crystalline U_3Si is rendered amorphous. Subsequently, the fission gas atoms and bubbles undergo motion in the flowing material. This motion has been qualitatively characterized by enhanced diffusivities given by Eqs. 21 and 22, respectively. If we assume an average dilatation, $3\Delta a/a$, of 3%, Eq. 21 predicts a diffusivity of about 6×10^{-14} m^2s^{-1}. This value for the gas atom diffusivity is equivalent to a viscosity of about 350 poises. The reader should note that the effective diffusivities (Eq. 21 and 22) used to characterize bubble motion in plastically flowing material are not related to the viscosity through the Stokes-Einstein equation (eq. 23). Although these diffusivities are characteristic of those within the "liquid-like" damage cascade regions, as discussed in Ref. 29, they are not observed in the bulk irradiated amorphous material. This apparent anomaly has been addressed by van den Beukel [34], where violations of the Stokes-Einstein relation (from linear to parabolic behavior) has been measured. The violation of the Stokes-Einstein relation is attributed to high concentrations of flow defects in irradiated amorphous materi-

als in response to applied stress.

Following the above discussion, GRASS-SST has been used to simulate fission gas behavior in U_3Si. The amorphous U_3Si was treated as if it were a low-melting-point (150°C) material. A gas atom diffusivity of 6×10^{-14} m^2s^{-1} was used, and bubbles were assumed to move by volume diffusion as given by Eq. 22. Figure 11 shows the GRASS-SST-calculated evolution of the gas-bubble size distribuiton in amorphous U_3Si. The calculations show that the bubble size distribution evolves to larger sizes as the irradiation proceeds. This results in an unrestrained fractional volume swelling of about 135% at 6×10^{27} fissions$\cdot m^{-3}$.

Although the bubble sizes calculated for amorphous U_3Si are substantially larger than those calculated for crystalline U_3Si_2, the model does not describe the extreme porosity and frothing observed in Fig. 2. This discrepancy is due to the absence of a realistic model to describe swelling in a material that exhibits plastic flow characteristic of a low viscosity. Small bubbles, formed from the precipitation of gas atoms, act as sinks for the continusously generated fission gas. The persistent radiation damage provides a sustained softening of the amorphous material. Upon bubble coalescence, the number of gas atoms and the bubble volume are conserved. Thus, these newly formed bubbles are in an over-pressurized state. Subsequently, the bubbles grow toward their equilibrium configuration by deforming the relatively soft surrounding material. Upon reaching equilibrium, the total surface area of the bubbles is conserved and a significant volume increase results.

IV. CONCLUSIONS

We have reviewed the irradiation behavior of intermetallic uranium alloys and have found similarities with the irradiation behavior of other intermetallics. Several of these systems undergo a crystalline-to-amorphous transformation during irradiation at low temperatures. The amorphous phases soften and are mechanically unstable during irradiation, even though they are brittle after irradiation. The mechanical instability arises from an elastic softening which increases the ductility by many orders of magnitude. In reactor fuels, this mechanical instability results in the rapid nucleation and growth of fission gas bubbles. Because of the decreased viscosity of the amorphous material under irradiation, fission-gas bubbles coalesce to form extremely large cavities, and the material swells at an uncontrollable rate (frothing). This swelling can be as much as three orders of magnitude greater than that observed in crystalline material.

Insight into the mechanisms involved has been gained through computer modeling with the GRASS-SST computer code. The kinetics of swelling in crystalline U_3Si_2 have been studied. The majority of fission gas is found to be in small bubbles (diameters <5 nm) which are dispersed throughout the crystal lattice. However, the swelling arises equally from the high density of small bubbles and a low density of large bubbles which are pinned to dislocations. Calculations show that the growth of the bubbles on dislocations is very sensitive to irradiation-induced re-solution of gas atoms from the bubble back into the crystal lattice. Re-solution from bubbles on dislocations is predicted to occur at a rate that is ten times lower than that from bubbles dispersed in the crystal lattice. This difference is due to a larger knock-out distance required to separate a gas atom from a bubble located on a dislocation. For gas atom knock-out distances less than the gas-capture radius for a dislocation, the gas associated with bubbles on dislocations is effectively trapped. Thus,

bubbles on dislocations are more effective at retaining their gas and grow at a higher rate than bubbles dispersed in the crystal lattice. The peaks in the bubble distribution at small and large sizes (Fig. 11) result from a balance between bubble nucleation, growth driven by diffusion, and shrinkage driven by re-solution (the latter two are linearly dependent on fission rate). Thus, the bubble size distribution is independent of fission gas generation rate but dependent on the total number of fission events or on the amount of gas generated. Changes in dislocation density or fuel chemistry during irradiation will strongly affect the distribution of large bubbles.

Analysis of fission gas behavior in irradiated amorphous U_3Si suggests that irraditaion softening combined with bubble overpressurization results in very large plastic flow. The effect of plastic flow has been modeled by an effective diffusivity. Enhanced diffusion leads to very rapid nucleation of gas bubbles, a rapid coarsening of the bubble-size distribution, and an enhanced fuel swelling rate. This model does not fully describe the observed extent of bubble growth and frothing, which arise from very rapid bubble migration and coalescence due to plastic flow.

APPENDIX

Coalescence between bubbles causes bubbles to change from one size class to another. The probability that a coalescence between an i bubble and a j bubble will result in a k bubble is given by the array T_{ijk}. Assume that $i \geq j$ in all cases. The number of gas atoms involved in one such coalescence is $S_i + S_j$. The array T_{ijk} is defined by the following three conditions:

1. The total probability of producing a bubble is unity; i.e., $\sum_k T_{ijk} = 1$.

2. The number of gas atoms, on the average, is conserved; i.e. $\sum_k T_{ijk} S_k = S_i + S_j$.

3. For a given pair, i and j, only two of the T_{ijk} array elements (corresponding to k and k + 1, where $S_k \leq S_i + S_j \leq S_{k+1}$; i.e, $m \geq 1.6$) can be nonzero.

From these three conditions, it follows that k = i, and

$$T_{ijk} S_k + (1 - T_{ijk}) S_{k+1} = S_i + S_j . \qquad \text{(A1)}$$

Thus, the probability that a coalescence between an i bubble and a j bubble results in a k bubble is given by

$$T_{ijk} = \frac{S_{k+1} - S_i - S_j}{S_{k+1} - S_k} = 1 - \frac{S_j}{S_{k+1} - S_k} . \qquad \text{(A2)}$$

The array T_{ijk} may be considered as the probability that an i bubble becomes a k bubble as a result of its coalescence with a j bubble. The rate N_{ik} at which i bubles become k bubbles is given by

$$N_{ik} = \sum_{j \le i} C_{ij} T_{ijk} . \qquad \text{(A3)}$$

The j bubble is assumed to disappear; gas atoms are absorbed into the i bubble. The rate x_x of disappearance is given by

$$x_j = \sum_{i \ge j} C_{ij} , \qquad \text{(A4)}$$

The rate N_{ik} at which i bubbles become k bubbles, with k = i+1, is reduced by re-solution of gas atoms. Re-solution is the rsult of a direct (or possibly indirect) collision between a fission fragment and a gas bubble. From Eqs. A2 and A3

$$N_{ik} = \sum_{j \le i} C_{ij} T_{ijk}$$

$$= \sum_{j \le i} P_{ij} F_i \frac{S_j}{S_k - S_i} \qquad \text{(A5)}$$

$$= \frac{F_i}{S_k - S_i} \sum_{j \le i} P_{ij} F_j S_j ,$$

The expression

$$\sum_{j \le i} P_{ij} F_j S_j ,$$

gives the rate at which gas atoms are added to an i bubble. Re-solution causes an i bubble to lose gas atoms at a rate given by $b_i S_i$, where b_i is the probability that a gas atom in an i bubble is redisolved. The reduced N_{ij} becomes

$$N_{ik} = \frac{F_i}{S_k - S_i} \left[\sum_{j \leq i} (P_{ij} F_j S_j) - b_i S_i . \right]. \qquad \text{(A6)}$$

If the expression within parentheses is negative, then N_{ik} is zero, and $N_{ik'}$, the rate at which i bubbles become i - 1 bubbles, with $k' = i - 1$, is

$$N_{ik'} = \frac{F_i}{S_i - S_{k'}} (b_i S_i - \sum_{j \leq i} P_{ij} F_j S_j). \qquad \text{(A7)}$$

Equations A6 and A7 are proportional to the probabilities that any particular i bubble becomes an i + 1 or an i - 1 bubble, respectively; the ratio of the probabilities is equal to the ratio of the rates. Clearly, the above definitions of N_{ik} converve the total number of gas atoms.

REFERENCES

1. Hofman, G. L., *Journal of Nuclear Materials*, Vol. 140, 1986, pp. 256-263.
2. Pellas, P., *Comptes Rendus Hebdomadaires des Seances de l'Academie des Sciences*, Vol. 233, 1969, pp. 1369-1371.
3. Niguib, H. M. and Kelly, R., *Radiation Effects*, Vol. 25, 1975, pp. 1-12.
4. Cartz, L. and Fournelle, R., *Radiation Effects*, Vol. 41, 1979, pp. 211-217.
5. Cartz, L., Karkoris, F. C., and Fournelle, R. A., *Radiation Effects*, Vol. 54, 1981, pp. 57-64.
6. Porter, D. L., Pascussi, M. R., and Olbert, B. H., *Journal of Nuclear Materials*, Vol. 103-104, 1981, pp. 767-772.
7. Fowler, J. D., Jr., Hurley, C. F., Kennedy, J. C., and Clinard F. W., Jr., *Journal of Nuclear Materials*, Vol. 103-104, 1981, pp. 755-760.
8. DeNatale, J. F. and Howitt, D. G., *American Ceramic Society, Bulletin*, Vol. 66, No. 9, 1987, pp. 1393-1396.
9. Klaümunzer, S., Schumacher, C., Rentzsch, S., and Vogel, G., *Acta Metallurgica*, Vol. 30, 1982, pp. 1493-1502.
10. Klaümunzer, S., and Schumacher, C., *Physical Review Letters*, Vol. 51, No. 21, 1983, pp. 1987-1990.
11. Klaümunzer, S., Schumacher, C., Hou, Ming-dong, and Vogel, C., *Rapidly Quenched Metals*, Vol. 1, S. Steeb and H. Warlimont, Eds., North Holland, New York, 1985.
12. Klaümunzer, S., Liu, Li Chang, and Schmacher, C., *Applied Physics Letters* (in press).
13. Bloch, J., *Journal of Nuclear Materials*, Vol. 6, 1962, pp. 203-212.

14. Coffinberry, A. S. and Waldron, M. B., *Progress in Nuclear Energy*, Vol. 1, 1956, p. 399.

15. Yeniscavich W. and Bleiberg, M. L., WAPD-BT-20.

16. Birtcher, R. C., Allen, C. W., Rehn, L. E., and Hofman, G. L., *Journal of Nuclear Materials*, Vol. 152, 1988, pp. 73-76.

17. Okomoto, P. R., Rehn, L.E., Pearson, J., Bhadra, R., and Grimsditch, M., In *Proc. Int. Symposium on Solid-State Amorphizing Transformations*, Los Alamos National Laboratory, August 1987, (in press).

18. Rest, J., *GRASS-SST: A Comprehensive, Mechanistic Model for the Prediction of Fission-Gas Behavior in UO_2-Base Fuels during Steady-State and Transient Conditi ons,* NUREG/CR-0202, ANL-78-53, Argonne National Laboratory, 1978.

19. Rest, J. and Cronenberg, A.W., *Journal of Nuclear Materials*, Vol. 150, 1987, pp. 203-225.

20. Hoh, A. and Matzke, Mj., *Journal of Nuclear Materials*, Vol. 48, 1973, pp. 157-164.

21. Dowling, D. M., White, R. J., and Tucker, M. O., *Journal of Nuclear Materials*, Vol. 110, No. 1, 1982, pp. 37-47.

22. Turnbull, J. A., *Journal of Nuclear Materials,* Vol. 38, 1971, pp. 203-212.

23. Greenwood, C. W., Foreman, A. J. E., and Rimmer, D. E., *Journal of Nuclear Materials*, Vol. 4, 1959, pp. 305-324.

24. Speight, M. V. and Greenwood, C. W., *Journal of Nuclear Materials*, Vol. 16, 1965, pp. 327-332.

25. Krishan, K., *Radiation Effects*, Vol. 66, 1987, pp. 122-155.

26. Okamoto, P. R., Rehn, L. E., Pearson, J., Bhadra, R., and Grimsditch, M., *Procedures of Materials Research Society Meeting*, Boston, Mass., Nov. 1987, (in press).

27. Grimsditch, M., Coray, K. E., Bhadra, R., Kampwirth, R. T., and Rehn, L. E., *Physical Review*, Vol. B35, 1987, p. 883.

28. Schulson, E. M., *Journal of Nuclear Materials*, Vol. 83, 1979, pp. 239-264.

29. Hahn, H., Averback, R. S., and Rothman, S. J., Physical Review Letters, Vol. 59, 1982, pp. 1930-1933.

30. Diaz de la Ruban, T., Averback, R. S., Benedek, R., and Kins, W.E., Physical Reveiw Letters, Vol. 59, 1987, pp. 1930-1933.

31. Flynn, C. P., *Physical Review,* Vol. 171, No. 3, 1960, pp. 682-698.

32. Brimhall, J. L., Kissinger, H. E., and Pelton, A. R., *Radiation Effects*, Vol. 90, 1985, pp. 241-258.

33. Bethune, B., *Journal of Nuclear Materials*, Vol. 40, 1971, pp. 205-212.

34. Van den Beukel, A., *Scripta Metallurgica*, Vol. 22, 1988, pp. 877-880.

LIST OF FIGURES

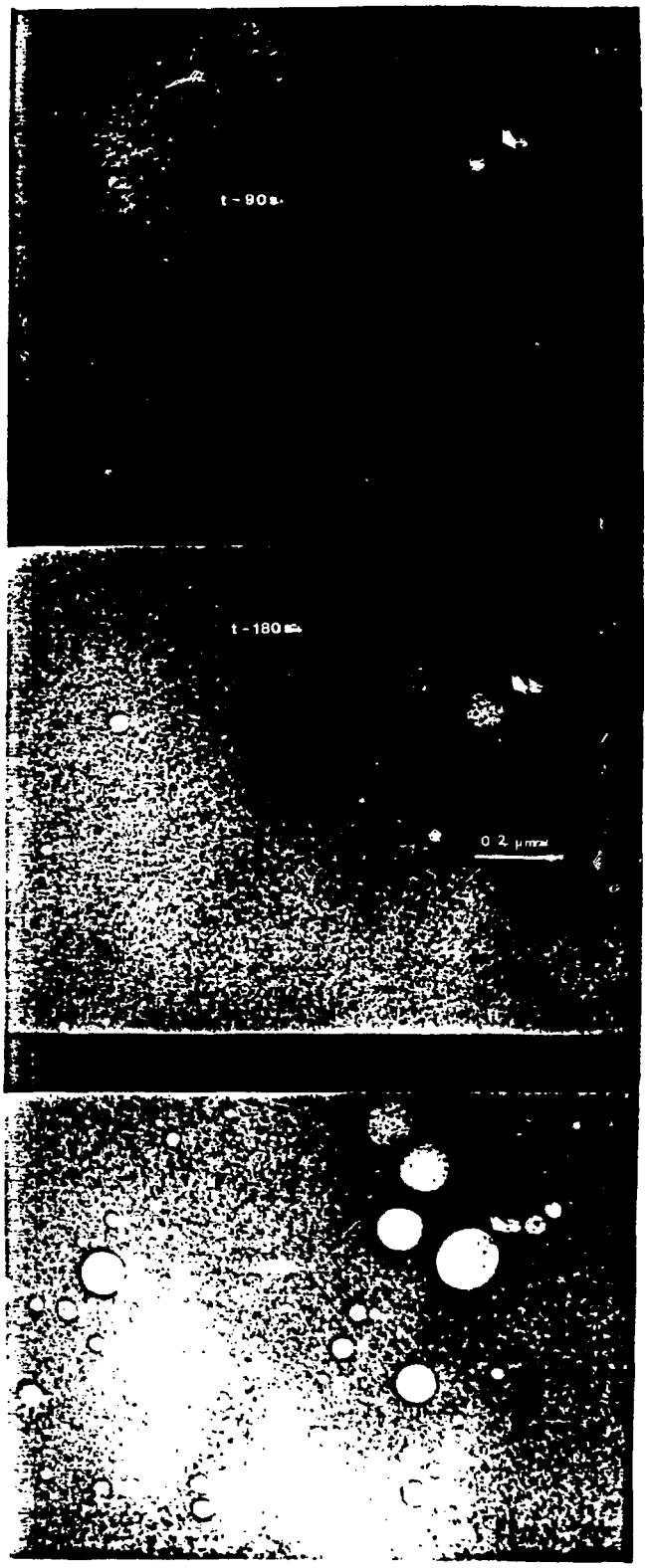

Fig. 1. Void and Bubble Growth in Preirradiated Boro Silicate Glass During Electron Irradiation

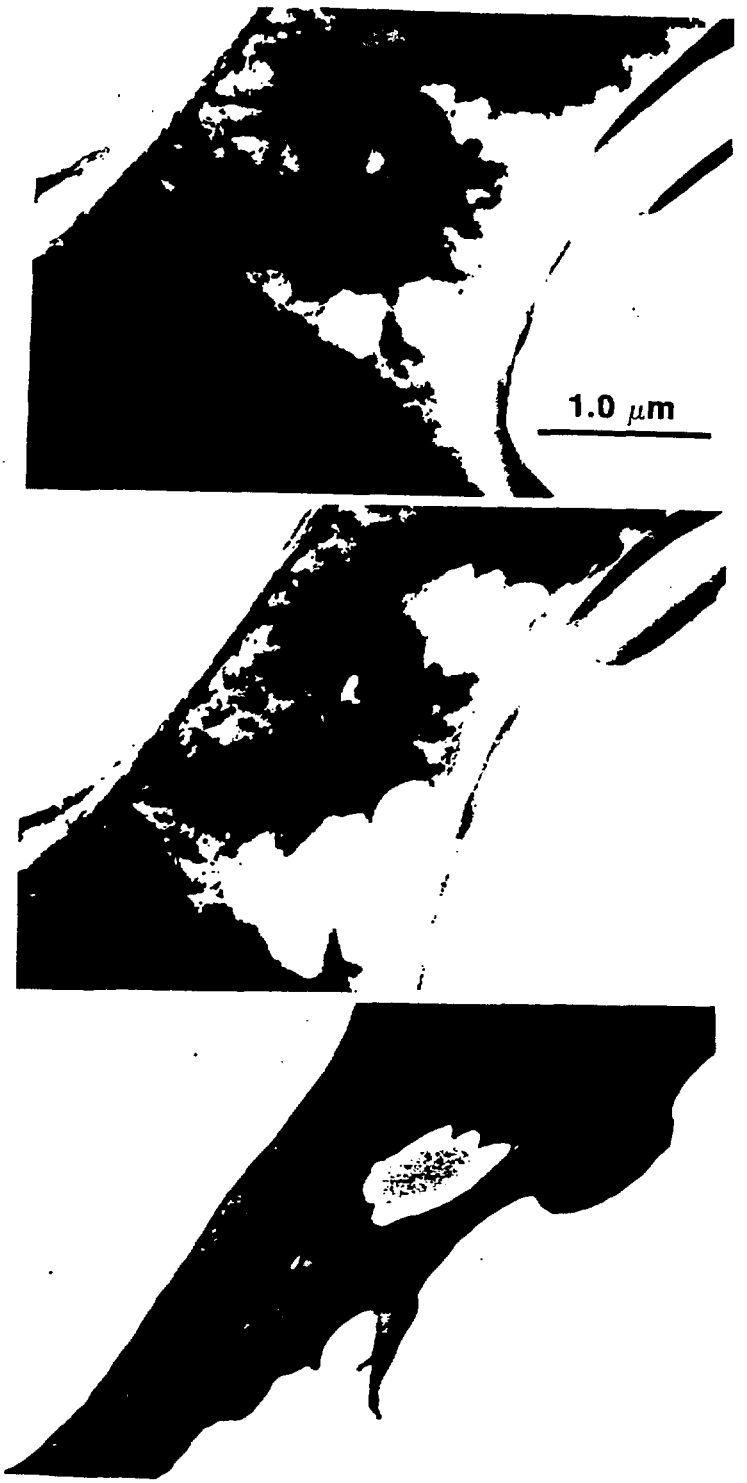

Fig. 3. Deformation U_3Si (Black) as
a Function of Kr Dose

Fig. 5. Scanning Microscope Image of the Surface
of a Large Bubble Shown in Fig. 2

UAl_x, FD 6 x 10^{21} cm^{-3}

U_3Si_2, FD 15 x 10^{21} cm^{-3}

U_3Si, FD 5 x 10^{21} cm^{-3}

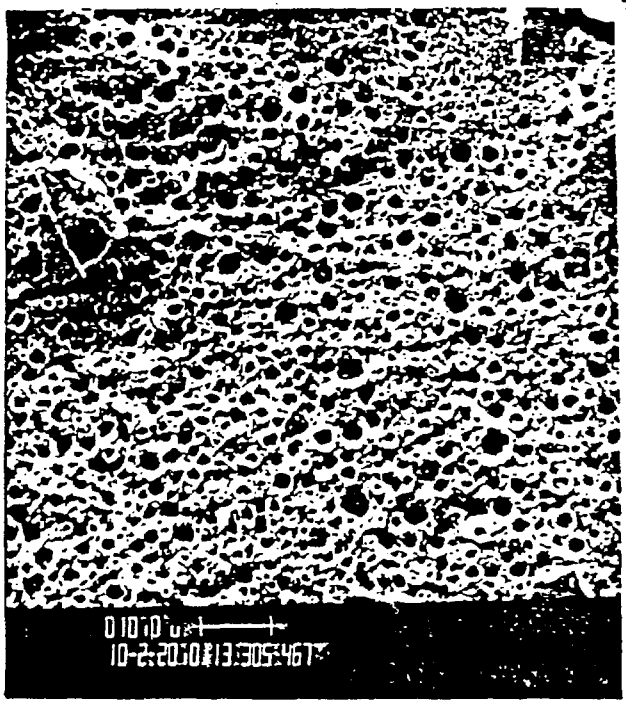

U_6Fe, FD 2 x 10^{21} cm^{-3}

Fig. 7. Characteristic Fission Gas Bubble Morphology in Various Intermetallic Uranium Compounds after Indicated Fission Density (FD)

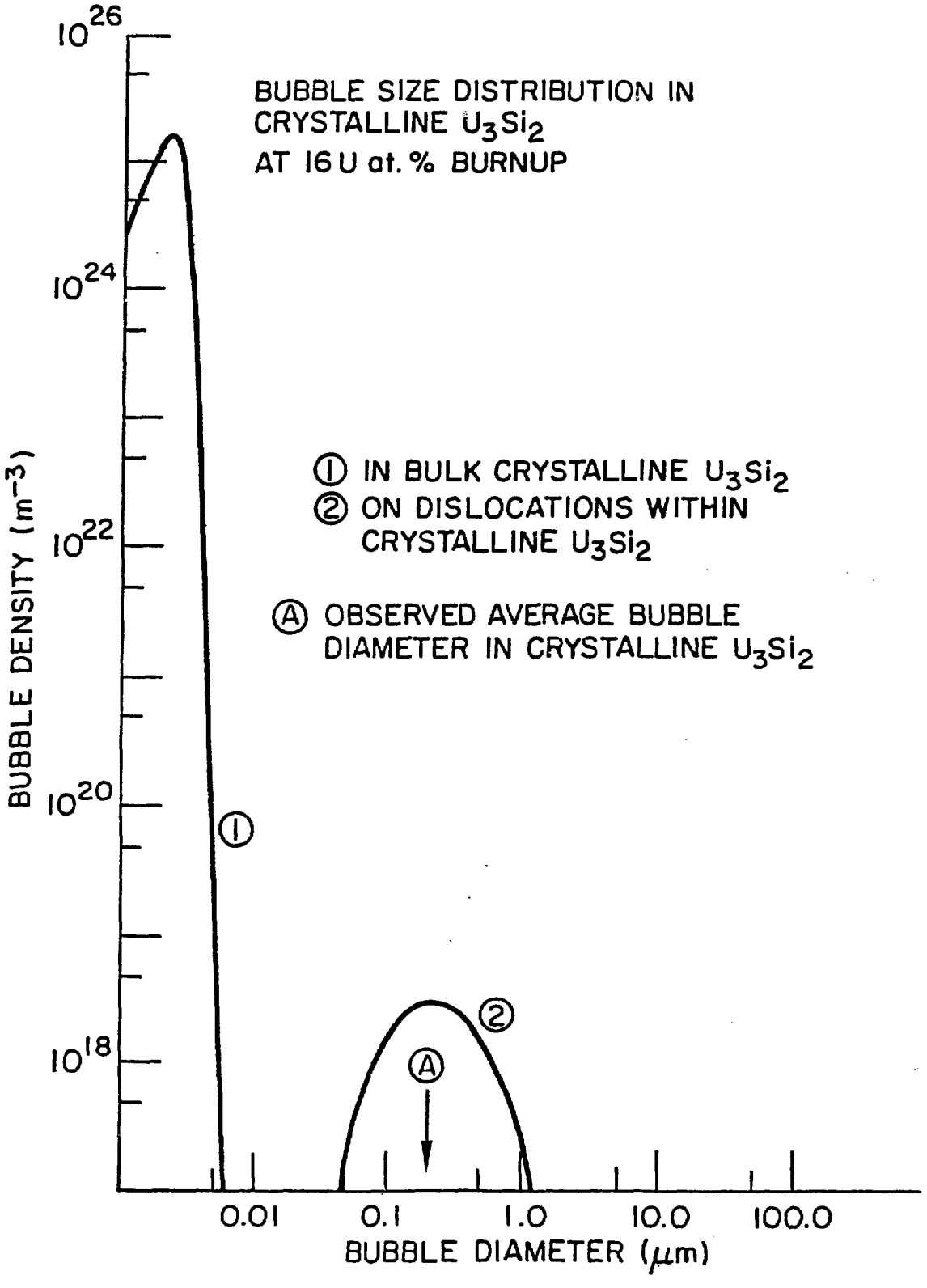

Fig. 9. Bubble Size Distribution in Crystalline U_3Si_2 at 16 at.% Burnup